Effect of the Emperor seamounts on trans-oceanic propagation of the 2006 Kuril Island earthquake tsunami

S. Koshimura,[1] Y. Hayashi,[2] K. Munemoto,[1] and F. Imamura[1]

Received 25 September 2007; revised 3 November 2007; accepted 13 December 2007; published 24 January 2008.

[1] The effect of tsunami wave scattering by the Emperor seamounts on the propagation of the 2006 Kuril Island earthquake tsunami is demonstrated, using the finite difference method. The model results indicate that the contribution of the Emperor seamounts on the maximum tsunami energy along the Pacific coast of Japan is found to be as much as 50% or more. Also, analysis of the spectral evolution of observed tsunami records in Japan suggests that the scattering waves from the Emperor seamounts possibly dominate the wave components at periods of 4 to 17 minutes. **Citation:** Koshimura, S., Y. Hayashi, K. Munemoto, and F. Imamura (2008), Effect of the Emperor seamounts on trans-oceanic propagation of the 2006 Kuril Island earthquake tsunami, *Geophys. Res. Lett.*, *35*, L02611, doi:10.1029/2007GL032129.

1. Introduction

[2] On 15 November, 2006, 11:14 (UTC), an earthquake of the moment magnitude 8.3 (USGS) occurred in the vicinity of Kuril Islands. A tsunami that accompanied this earthquake propagated across the entire Pacific Ocean. Although no devastating damage or casualties from the tsunami were reported, this tsunami showed extraordinary features during its propagation in the northern Pacific. According to *Japan Meteorological Agency* (*JMA*) [2006], at 22 of 70 tide stations along the Pacific coast of Japan, the maximum tsunami heights occurred more than 5 hours after the primary wave arrived. Generally, possible causes for the long duration of tsunami oscillations have been trapped mode of edge waves on continental shelf and scattering waves from seamounts. In particular, *Mofjeld et al.* [2001] pointed out that topographic features of the Pacific Ocean interacts with tsunami as it passes by, creating interference patterns of scattering waves.

[3] The present study aims to determine the effect of scattering waves on the trans-oceanic propagation of the 2006 Kuril Island earthquake tsunami toward the Pacific coast of Japan. First, the authors perform numerical modeling, and comprehend the tsunami propagation features in the northern Pacific and the contribution of scattering waves from the Emperor seamounts on the tsunami energy along the Pacific coast of Japan. Second, through the spectral evolution analysis of observed tsunami records in Japan, the frequency response of the scattering waves from the Emperor seamounts is discussed.

[1]Disaster Control Research Center, School of Engineering, Tohoku University, Sendai, Japan.
[2]Meteorological Research Institute, Tsukuba, Japan.

0094-8276/08/2007GL032129$05.00

2. Numerical Modeling

[4] For the modeling of trans-oceanic propagation of tsunami, we use the finite difference method of the linear shallow-water wave theory with Coriolis force in a spherical coordinate system, which was primarily developed by *Nagano et al.* [1991]. The computational domain is shown in Figure 1a with corner coordinates (5.0°S, 120.0°E) and (60.0°N, 250.0°E). We use the digital bathymetry data (GEBCO) distributed by *British Oceanographic Data Centre* [1997] for tsunami modeling. The spatial grid size is 1-arc-minute (approximately 1800 m) and the time step is 3 seconds to satisfy the stability condition. We apply the total reflection condition at the boundary between land and sea, and the free radiation condition at the open-ocean boundary.

[5] As the initial condition, we assume instantaneous displacement of the sea surface identical to the vertical sea floor displacement shown in Figure 1b. The vertical sea floor displacement field for a rectangular fault model is computed by using the theory of *Mansinha and Smylie* [1971]. The fault parameters are determined by considering the teleseismic body wave inversion analysis of *Yamanaka* [2006], the aftershock distribution and tectonic setting: fault length = 200 km, fault width = 60 km, (strike, dip, slip) = (220°, 25°, 96°), and average slip = 5.8 m. The resulting seismic moment is calculated to be $M_0 = 2.088 \times 10^{21}$ Nm ($M_w = 8.14$), assuming a uniform shear modulus $\mu = 3.0 \times 10^{10}$ N/m^2. The maximum uplift and subsidence are calculated to be 2.91 m and 0.62 m respectively.

[6] Figure 2 shows the snapshot of modeled tsunami passing by the Emperor seamounts at 3 hours after the earthquake. As the leading tsunami phase passes by sharp changes in bathymetry, some wave patterns like concentric circles are found at the Emperor seamounts.

[7] The model results are validated by comparison with observed tsunami records from JMA tide gauges and NOAA's DART buoys [e.g., *NOAA Center for Tsunami Research*, 2006], as shown in Figure 3. The modeled tsunami waveforms are reasonably consistent with the observed tsunami waveforms in terms of the arrival of primary wave, its amplitude and frequency. However, note that the waveforms in the later phase may not be well resolved because the present model is based on the linear shallow water theory. For more precise discussion, the dispersive wave theories such as Boussinesq equations may be required.

3. Effect of the Emperor Seamounts on Tsunami Propagation

[8] The contribution of the Emperor seamounts on tsunami energy along the Pacific coast of Japan is assessed by

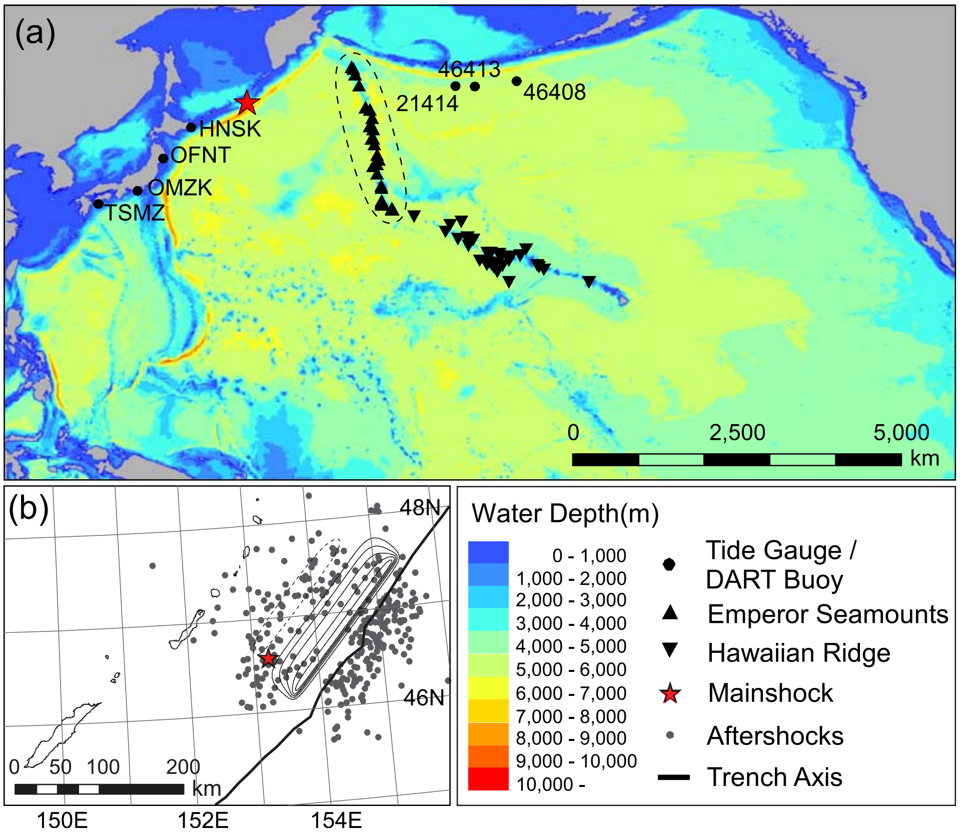

Figure 1. (a) Bathymetry of the northern Pacific. Triangles indicate the Emperor seamounts (the area circled by dashed line) and Hawaiian Ridge. Black dots are the points for model output. Abbreviations are as follows: HNSK = Hanasaki, OFNT = Ofunato, OMZK = Omaezaki, and TSMZ = Tosashimizu for JMA tide gauges, and 21414, 46413, and 46408 are for DART buoys of NOAA. (b) Computed coseismic displacement of sea bottom due to the 2006 Kuril Island earthquake. The contour interval is 0.5 m. Solid lines are for uplift, and a dashed line is for subsidence. The gray dots indicate the epicenter of aftershocks within 24 hours since the main shock occurred.

the numerical modeling with a hypothetical bathymetric grid created by eliminating the Emperor seamounts, i.e., a flat sea bottom taking the place of the actual topography of it (approximately 5000 m in the circled area with dashed line in Figure 1a). Eliminating the Emperor seamounts on the model results is shown in Figure 4. This is a comparison of modeled waveforms at Ofunato and Omaezaki by using original GEBCO grid and the hypothetical one described above. It is inferred that the effect revealed as decreased tsunami heights at later times within the wave train (after 300 minutes at Ofunato and 400 minutes at Omaezaki), by the absence of scattering waves from the Emperor seamounts. After the validation of tsunami travel time based on the ray-tracing method [e.g., *Satake*, 1988], we regard these times (300 and 400 minutes) as the approximate arrival time of scattering wave at Ofunato and Omaezaki, respectively.

[9] Here, we introduce an energy contribution index E_C defined as

$$E_C = \frac{E_R - E_H}{E_R} \tag{1}$$

where E_R is maximum tsunami energy flux calculated at each computational grid with real bathymetry (original GEBCO grid), and E_H is with the hypothetical bathymetry which eliminates the topography of the Emperor seamounts. E_R and E_C are defined as the averaged energy flux of progressive long wave in a unit area of the free surface [e.g., *Dean and Dalrymple*, 1984],

$$E = \frac{\rho g \eta^2}{2} \cdot \sqrt{gh} \tag{2}$$

where ρ is the density of water, η is the maximum water level calculated at each computational grid, and h is local water depth at each grid. $E_R - E_H$ is the difference of computed maximum tsunami energy flux of two bathymetry scenarios, and is interpreted as the net amount of scattering wave energy. Thus, taking the ratio of $E_R - E_H$ to E_R can be evaluated as the contribution of the Emperor seamounts on the maximum tsunami energy. Figure 5 illustrates the spatial distribution of E_C calculated for the area shallower than 100 m in water depth, along the Pacific coast of Japan. This suggests that the contribution of the Emperor seamounts is as much as 50% or more of the tsunami energy arriving at the Pacific coast of Japan.

4. Discussions on Spectral Evolution of Observed Tsunamis

[10] In order to determine whether any significant change in the observed tsunami can be recognized during the

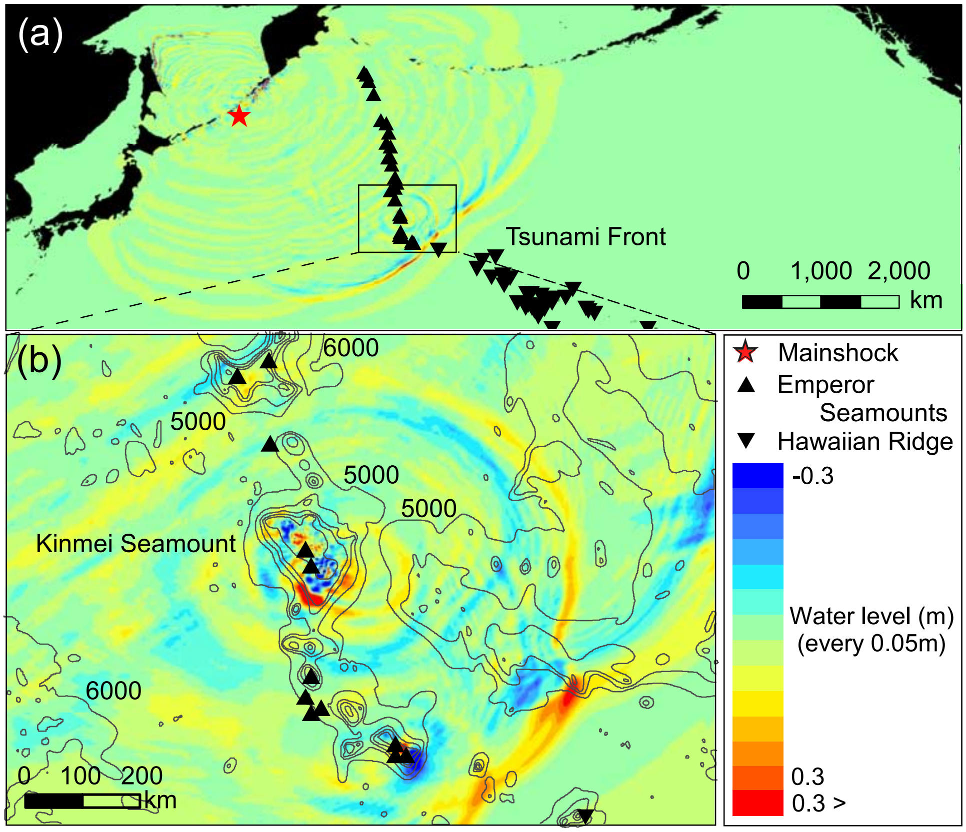

Figure 2. (a) Snapshot of modeled tsunami propagating in the northern Pacific 3 hours after the earthquake occurred. (b) Scattering wave excited by Kinmei seamount. The contour with gray line denotes the sea bottom topography (water depth) around Kinmei seamount. The contour interval is 1000 m.

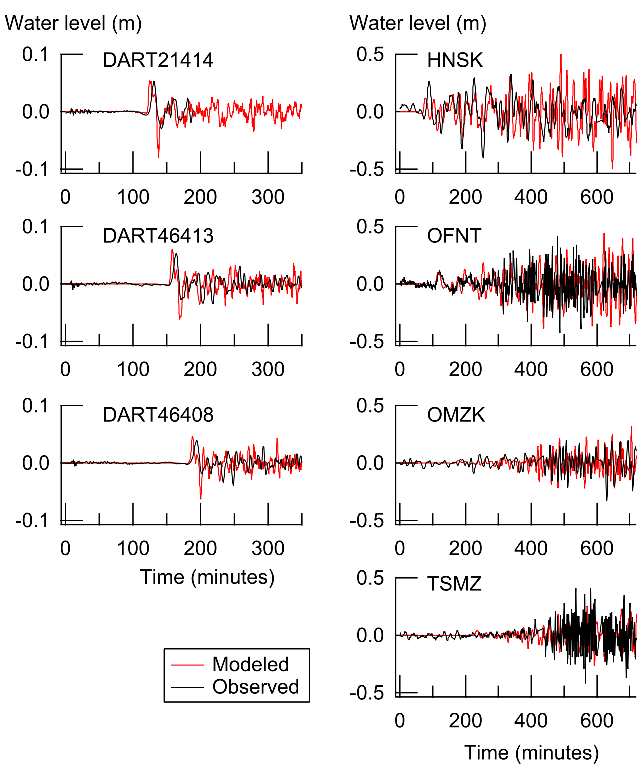

Figure 3. Comparison of the modeled waveforms with observed tsunami records from four JMA tide gauges along the Pacific coast of Japan and at three DART stations (21414, 46413, and 46408). The plots start at the origin time of the earthquake.

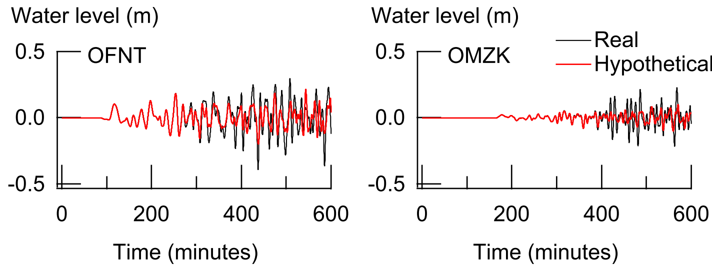

Figure 4. Comparison of modeled waveforms at Ofunato and Omaezaki obtained with two bathymetry scenarios. The black solid line indicates the modeled waveform with original GEBCO grid, and the red line indicates the modeled waveform with a hypothetical bathymetric grid.

passage of scattered waves, the spectra along a moving time-window of 128 data points are calculated using the data at Ofunato and Omaezaki, sampled every 1 minute at JMA tide gauge. Figure 6 shows the spectra for four spectral periods of 33–67, 17–33, 8–17 and 4–8 minutes. The abrupt change of Fourier components is evident in two bands of 8–17 and 4–8 minutes (blue and green lines in Figure 6) occurs at 300–400 minutes, coincident with the arrival time of scattering waves from the Emperor seamounts.

[11] Also, the Fourier spectra of observed tsunamis are calculated for two separated durations of each record (Figure 7); the records of 100–300 and 300–500 minutes at Ofunato, and 150–400 minutes and 400–650 minutes at Omaezaki. In theory, as *Rabinovich* [1997] suggested, the observed tsunami include the wave components associated with both topography and tsunami source. The approximate dominant period affected by tsunami source can be estimated as,

$$T_n = \frac{2L}{n\sqrt{gh}}, \quad n = 1, 2, \ldots \qquad (3)$$

where L is the dominant horizontal scale of the tsunami source, g is the acceleration of gravity, and h is the mean water depth within the tsunami source area. From Figures 1 and 2a, the first phase of the tsunami toward the Pacific coast of Japan is likely to be dominated by the component of major axis of the tsunami source. Then, T_1 = 32.2 (min.) is calculated (L = 200 km, h = 4375 m) as the typical period of tsunami source component which might be observed at Ofunato and Omaezaki, and it is consistent with the spectral peaks of approximately 30 minutes shown in Figure 7. Therefore, the spectral peaks of 4 to 17 minutes in the later

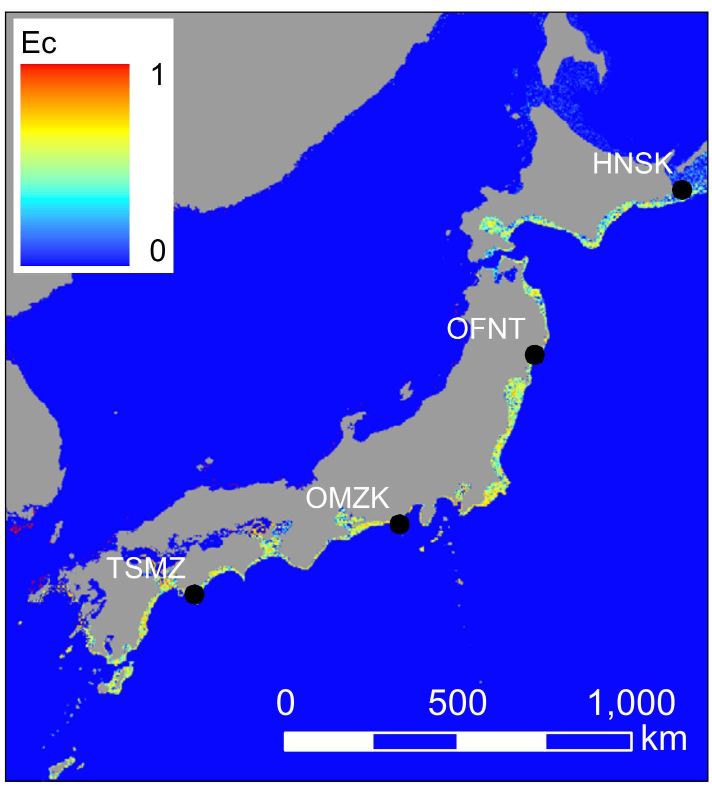

Figure 5. Spatial distribution of E_C as the contribution of the Emperor seamounts on maximum tsunami energy. Note that E_C is visualized only for the area shallower than 100 m in water depth along the Pacific coast of Japan.

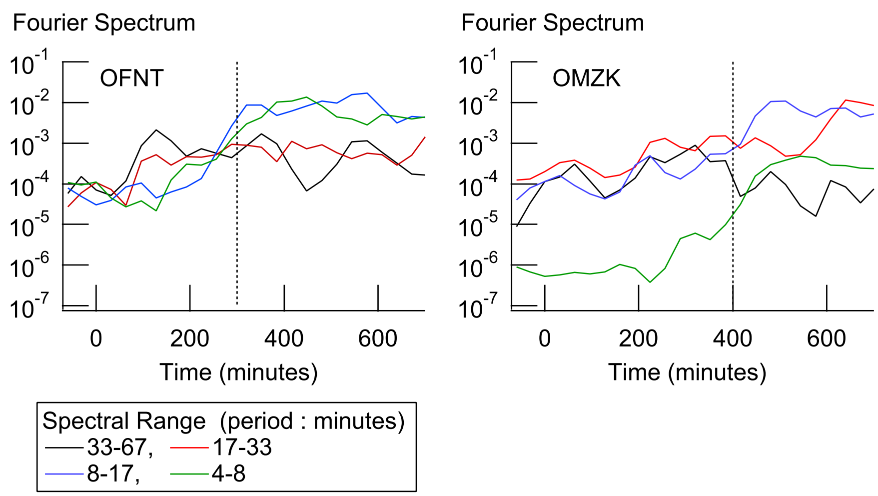

Figure 6. Time evolution of Fourier spectra of observed tsunami records at (left) Ofunato and (right) Omaezaki. $t = 0$ indicates origin time of the earthquake. The vertical dashed lines indicate the arrival time of scattering waves from the Emperor seamounts interpreted from Figure 4.

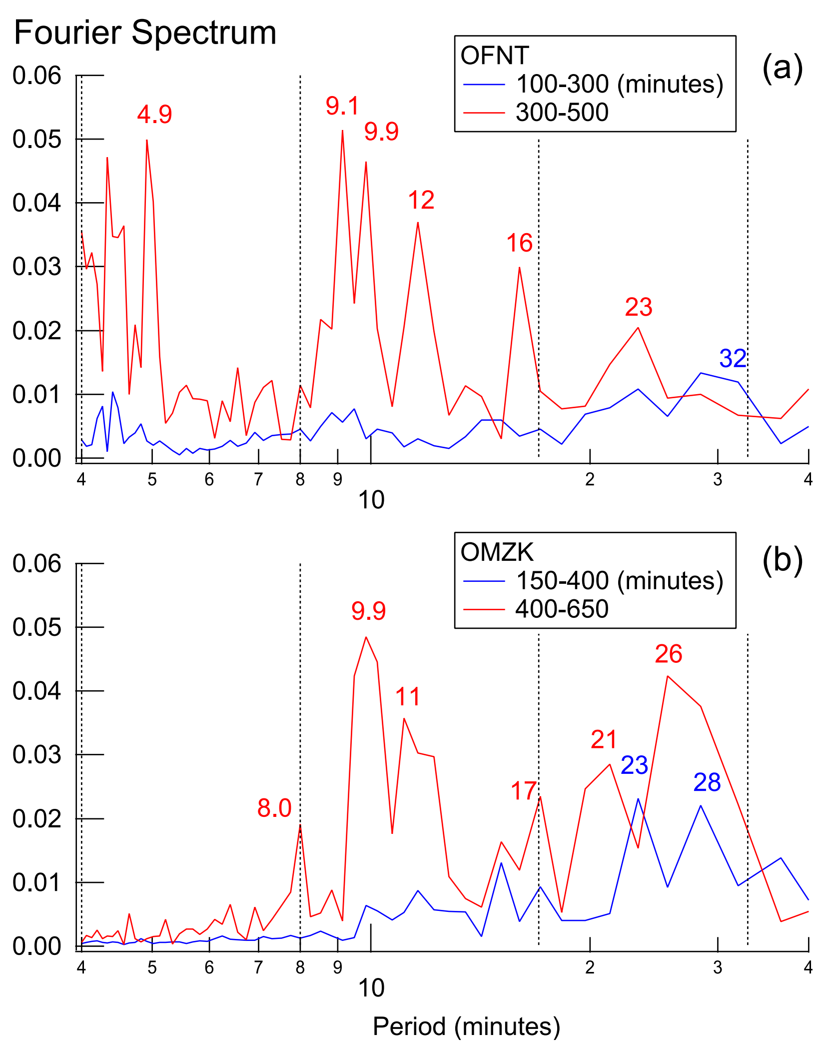

Figure 7. Fourier spectra calculated for two separated durations: (a) the records of 100–300 and 300–500 minutes at Ofunato(OFNT) and (b) 150–400 minutes and 400–650 minutes at Omaezaki(OMZK). Numerals in the figures denote the peak periods (in minutes).

phase of tsunami records (after 300–400 minutes) can be interpreted as the wave components scattered by the Emperor seamounts, according to the results shown in Figure 6.

[12] **Acknowledgments.** The present study was funded in part by Grant-in-Aid for Scientific Research (Grant 19681019, 18254002) of The Ministry of Education, Culture, Sports, Science and Technology, Japan.

References

British Oceanographic Data Centre (1997), *The Centenary Edition of the GEBCO Digital Atlas* [CD-ROM], Liverpool, U. K.

Dean, R. G., and R. A. Dalrymple (1984), *Water Wave Mechanics for Engineers and Scientists*, *Adv. Ser. Ocean Eng.*, vol. 2, 353 pp., World Sci., Hackensack, N. J.

Japan Meteorological Agency (JMA) (2006), Monthly report on earthquakes and volcanoes in Japan, November 2006 (in Japanese), pp. 37–45, Tokyo.

Mansinha, L., and D. E. Smylie (1971), The displacement fields of inclined faults, *Bull. Seismol. Soc. Am.*, *61*, 1433–1440.

Mofjeld, H. O., V. V. Titov, F. I. Gonzalez, and J. C. Newman (2001), Tsunami scattering provinces in the Pacific Ocean, *Geophys. Res. Lett.*, *28*, 335–337.

Nagano, O., F. Imamura, and N. Shuto (1991), A numerical model for far-field tsunamis and its application to predict damages done to aquaculture, *Nat. Hazards*, *4*, 235–255.

NOAA Center for Tsunami Research (2006), Deep-ocean assessment and reporting of tsunamis, http://nctr.pmel.noaa.gov/Dart/, NOAA, Seattle, Wa.

Rabinovich, A. B. (1997), Spectral analysis of tsunami waves: Separation of source and topography effects, *J. Geophys. Res.*, *102*, 12,663–12,676.

Satake, K. (1988), Effects of bathymetry on tsunami propagation: Application of ray tracing to tsunamis, *Pure Appl. Geophys.*, *126*, 27–36.

Yamanaka, Y. (2006), Kuril Islands earthquake (2006/11/15), *EIC Seismol. Note 183*, Earthquake Res. Inst., Univ. of Tokyo, Tokyo. (Available at http://www.eri.u-tokyo.ac.jp/sanchu/Seismo_Note/2006/.)

Y. Hayashi, Meteorological Research Institute, Tsukuba, 305–0052 Japan.

F. Imamura, S. Koshimura, and K. Munemoto, Disaster Control Research Center, School of Engineering, Tohoku University, Sendai, 980–8579 Japan. (koshimura@tsunami2.civil.tohoku.ac.jp)